Numerical analysis of slot die coating of nanocellulosic materials

FUAAD PANIKAVEETIL AHAMED KUTTY, RAJESH KOPPOLU, AGNE SWERIN, FREDRIK LUNDELL, AND MARTTI TOIVAKKA

ABSTRACT: Nanocellulosic coatings as a food packaging material are of commercial interest due to their nontoxic nature, renewability, and excellent barrier properties. Complex shear-thinning rheology poses challenges in designing and sizing equipment to pump, mix, and process the suspension and actual coating process.

This study aims to determine the effectiveness of computational fluid dynamics (CFD) in predicting nanocellulosic suspension flow in light of existing rheological data. We employ and compare three distinct rheological models to characterize the rheology and flow of nanocellulose suspensions through a slot die coater, where the model parameters are established from existing slot rheometry measurements. A volume-of-fluid (VoF) based finite volume method is employed to simulate the flow in a slot die operated in an unconventional metering mode. Results with the Casson model predict the presence of unyielded regions in the flow, which was not captured using the power law model. These stagnation regions will incur coatability issues stemming from flow intermittencies and lead to potential defects in the coating layer, including fracture. The results suggest that a rheological model that includes yield stress should be considered while modeling such flows. A need for better rheological data to model nanocellulosic flows, especially at high consistencies and shear rates, is also highlighted.

Application: This work identifies and clarifies the challenges to be addressed when considering industrial scale nanocellulose coating of paperboard.

There is a compelling urgency to replace nonrenewable fossil fuel-based materials to reduce petroleum resource exploitation and adapt to more stringent environmental regulations. Cellulose fiber, found in plant cell walls and typically implanted into hemicelluloses and lignin matrices, is a bio-based building block with versatile applications. Micro- or nanostructured cellulosic fiber materials [1] reveal novel possibilities to replace conventional fossil fuel-based materials. Following proposed new TAPPI Standard WI 3021 "Standard terms and their definition for cellulose nanomaterial," cellulose nanomaterials are primarily grouped into nano-objects and nanostructured materials, depending on the resulting fibril features [2]. Cellulose nano-objects are relatively small and further classified as the cellulose nanofibrils (CNF) and cellulose nanocrystals (CNC). CNC possess relatively low width and low aspect ratio (3–10 nm and L/D > 5) compared to CNF (5–30 nm and L/D > 50). In contrast, the cellulose nanostructured materials are classified as cellulose microfibrils (CMF) and cellulose microcrystals (CMC). Among these, CMF is a heterogeneous mixture of nanofibrils, longer fibers, fibrillary fines, fiber fragments, and cellular remnants derived from the mechanical or chemical breakdown of the hierarchical structure of cellulose fibers [3]. Also, they maintain a high aspect ratio and are present as entangled networks with widths varying between 10–100 nm, with the corresponding lateral dimension extending up to a few microns. On the other hand, cellulose microcrystals (CMC) are short, relatively low aspect ratio (L/D < 2), rigid, and with a typical width of 10–15 µm. Microfibrillar cellulose (MFC) is another term for cellulose microfibrils produced from purely mechanical processes [4]. Such mechanically fibrillated material is particularly crucial in the circular bio-economy, as it classifies as unmodified natural polymers and is usually under the purview of "not chemically modified" substances. The excellent physical properties of MFC, deriving from their peculiar molecular arrangement, have driven significant interest in numerous future applications [5]. The possible end uses identified range from rheology modifiers, membrane filters, reinforcement additives, and binders for composites to barrier and functional coatings. The biodegradable [6] nature of nanocellulosic films, as well as their nontoxicity [7], good compatibility with several other materials, and excellent barrier properties [8] against grease, oils, and oxygen, make them particularly suited for food packaging applications [9].

Several researchers have developed methods to coat nanocellulose onto various substrates, targeting properties such as barriers, strength, printing, and other functionalities. Filtration on a polyamide filter cloth was one of the earliest reported techniques to produce MFC films [10]. Methods such as filtration and deposition [11], rod/bar coating [12], blade coating [13], spray-coating [14], and drawdown coating [15] have been employed to coat nanocellulosic materials onto a substrate. Although these techniques successfully managed coatings, the large viscosities [16] of

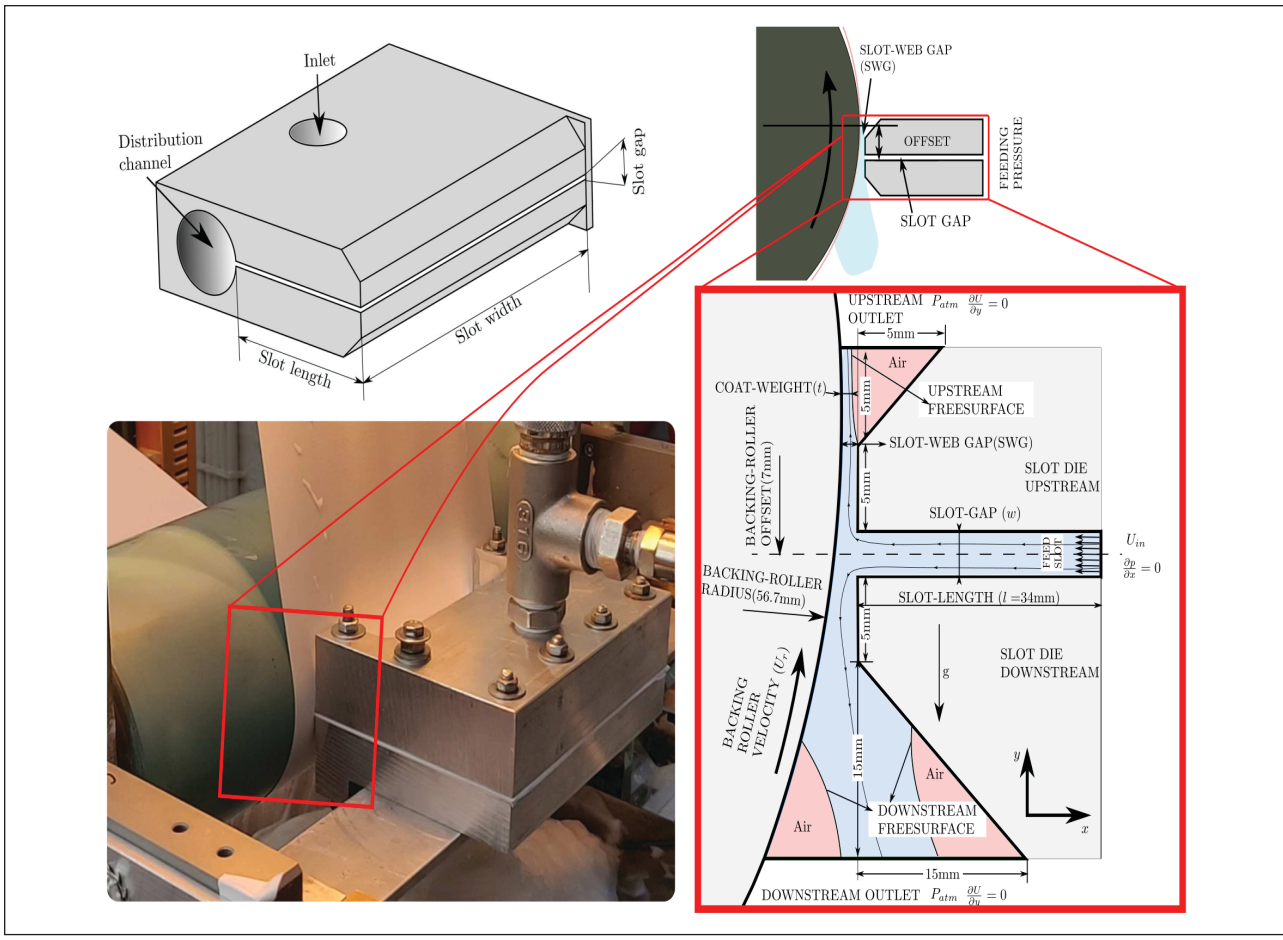

1. Slot die coating in metering mode (left), and corresponding simulation geometry and boundary conditions (right).

the suspensions at already low solids content limit the applied coat weight, necessitating multiple layers for reliable barrier properties. Removing a considerable amount of water at lower consistencies presents excessive drying demands, reducing these methods to laboratory-scale batch processes. Continuous roll-to-roll coating at sufficient coat weights is a prerequisite for large-scale commercial production. Guezennec et al. [17] realized coatings using a blend of PVOH and MFC with a blade coater onto paperboard at a comparatively moderate speed of 70 m/min. Later, higher speeds of 500 m/min were achieved using an inclined jet in the wire section of a paper machine to apply a thick layer of a MFC-mineral pigment composite on a draining paperboard web [18]. Mousavi et al. [13] applied CNF suspension onto the surface of paperboards in a batch process at 600 m/min using a cylindrical laboratory coater equipped with a pond applicator and a metering blade. In addition, there have been studies [19] describing the coating of cellulose nanocrystals on PET substrate using the reverse gravure method for optical and printing applications. Kumar et al. [20] developed a technique that enables continuous coating of MFC suspensions onto paperboard using a custom-built slot die on a modified mini pilot scale coater. They were able to achieve high coat weights, over 10 g/m² with 2 wt% consistency. According to the authors, the benefit of using the slot die is the possibility to create high deformation rates in the slot gap to fluidize the otherwise highly viscous nanocellulose suspension. Coat weight control was provided by running the slot die in an unconventional metering mode in which the trailing lip–paper gap controls the coat weight.

The complex rheological behavior of MFC suspensions is a challenge when coating paper, paperboard, and other substrates. The suspensions are highly shear thinning, with power law indexes typically in the range 0.1–0.3, and they exhibit considerable yield stress [21,22]. For example, Nazari et al. reported over 1000 Pa in yield stress for consistencies above 6% [21]. The high surface area resulting from exhaustive fibrillation, accompanied by the wide availability of hydroxyl groups on fibril surfaces, results in a high water holding tendency, which can slow down the drying of the applied wet coating layers [23]. The broad inhomogeneity present at the microscale distinguishes the MFC suspensions from their passive, gel-type counterparts—the so-called isotropic nanoparticle suspensions. The presence of large fibrils in MFC suspensions can lead to water release, resulting in, for example, water-rich boundary layers and apparent boundary slip in the flow [24]. These peculiar

properties create challenges in, for example, pumping, emptying vessels, stagnation of flow in coating devices, and poor film formation.

Some of the issues detailed previously can be addressed through experimental studies. However, when designing an appropriate coating apparatus for a given nanocellulose material and end-use application, the traditional trial and error approach of using the existing coating technology is expensive and slow. The unusual rheological properties and unknown flow behavior created by it leads to considerable uncertainty and risks in large-scale trials. More importantly, experimental trials seldom provide knowledge on the mechanisms that control the material's behavior and its processability into coatings; if a trial fails, it does not necessarily provide answers on how to proceed. The current work aims to understand, through mathematical modeling and numerical simulations, the mechanisms that control the flow of MFC suspensions during slot die coating.

PROBLEM FORMULATION

Computational fluid dynamics (CFD) has been extensively employed by several researchers to investigate flow phenomena in slot die coating, and operational windows have been successfully predicted for simple fluids [25,26]. The slot die is ordinarily operated in a premetered curtain or bead mode. However, in the current work, the simulation parameters are chosen from the previously reported experimental work [20] in which the slot die was successfully operated in the unconventional metering mode. **Figure 1** shows the slot die coating setup, the geometry and the boundary conditions for the computational domain, and the base case parameter values, which approximately correspond to the experimental work by Kumar et al. [20]. Here, the slot die coating head is placed at a 3 o'clock position about the backing roll and slightly offset downwards from the backing roll center position. Such an arrangement creates a converging geometry between the coating head lip and the backing roll that allows the coat weight to be controlled by the minimum gap between the top lip of the slot die and the substrate to be coated. In this metering operational mode, the excess coating falls downwards, is gathered, and can be reused. The metering off enables control of coat weight independently of the slot die feed flow rate, which is not possible with the standard premetered operational mode of slot die coating. This is advantageous when coating nanocellulosic materials, because high flow rates can be used to overcome the typical high yield stress of these materials to fluidize them. Low flow rates can result in unyielded, stagnated regions in flow. However, if a coater has sufficient drying capacity for the web speed required by the inflow, or the coating layer is very thin, metering off is not needed. In this case, the coat weight is controlled by the ratio of the web speed to the volumetric inflow into the slot die.

For simplicity, the substrate considered here is a non-absorbing, smooth surface on the backing roll surface. The surface roughness of the substrate and absorption of the liquid phase onto it can be important and should be considered in the future. A two-dimensional, laminar, steady-state flow field is assumed throughout the study. The governing partial differential equations (PDEs) for an incompressible, isothermal fluid can be expressed as the conservations of mass and momentum:

$$\nabla \cdot \boldsymbol{U} = 0 \tag{1}$$

$$\frac{\partial \rho_b \boldsymbol{U}}{\partial t} + \nabla \cdot (\rho_b \boldsymbol{U}\boldsymbol{U}) = -\nabla p + \rho_b \boldsymbol{g} + \nabla \cdot (2\mu_b \boldsymbol{S}) + \sigma\kappa(\nabla\alpha) \tag{2}$$

Here, $\boldsymbol{U}$ is the velocity field, t is the time, p is the pressure, and g is the acceleration due to gravity. Also, $\boldsymbol{S}$ is the mean strain rate tensor given by $\boldsymbol{S} = 0.5(\nabla\boldsymbol{U} + \nabla\boldsymbol{U}^T)$. The last term in Eq. 2 accounts for the surface tension effects and is modeled using the continuum surface force (CSF) method [27]. Here, σ is the coefficient of surface tension, and κ is the local surface curvature of the interface defined as:

$$\kappa = \nabla \cdot \left(\frac{\nabla\alpha}{|\nabla\alpha|}\right)$$

The bulk density ρ_b and viscosity μ_b are computed based on the weighted averaged distribution of the fluid fraction α as:

$$\rho_b = \rho_1\alpha + \rho_2(1-\alpha)$$

$$\mu_b = \mu_1\alpha + \mu_2(1-\alpha)$$

where μ_i and ρ_i are the densities and viscosities of the corresponding phase i. Also, the fluid fraction is advected as:

$$\frac{\partial\alpha}{\partial t} + \nabla.(\alpha\boldsymbol{U}) = 0 \tag{3}$$

The volume-of-fluid (VoF) method [28] captures the development of the free surface of the immiscible two-phase flow between the coating fluid and air. The finite volume method-based OpenFOAM framework is employed to discretize the system of PDEs resulting from the governing equations. More details on the solver implementation can be found in the documentation of interFoam [27] solver.

The rheology of nanocellulose is numerically described using three rheological models, as shown in **Fig. 2**. Apart from the Newtonian case, where the viscosity is assumed to be constant ($\tau = \mu\dot{\gamma}$), the power-law ($\tau = K\dot{\gamma}^n$) and Casson models ($\sqrt{\tau} = \sqrt{\tau_0} + \sqrt{\eta_p\dot{\gamma}}$)—the latter of which includes yield stress—are also implemented to characterize the rheology. The Casson model parameters were established from slot viscometry measurements reported for a 3% concentration of mechanically produced cellulose nanofibrils by Kumar et al. [22]. The power law indexes in the range 0.1–0.3 were chosen to envelop the experimental data in order to understand the influence of shear thinning behavior. The Casson

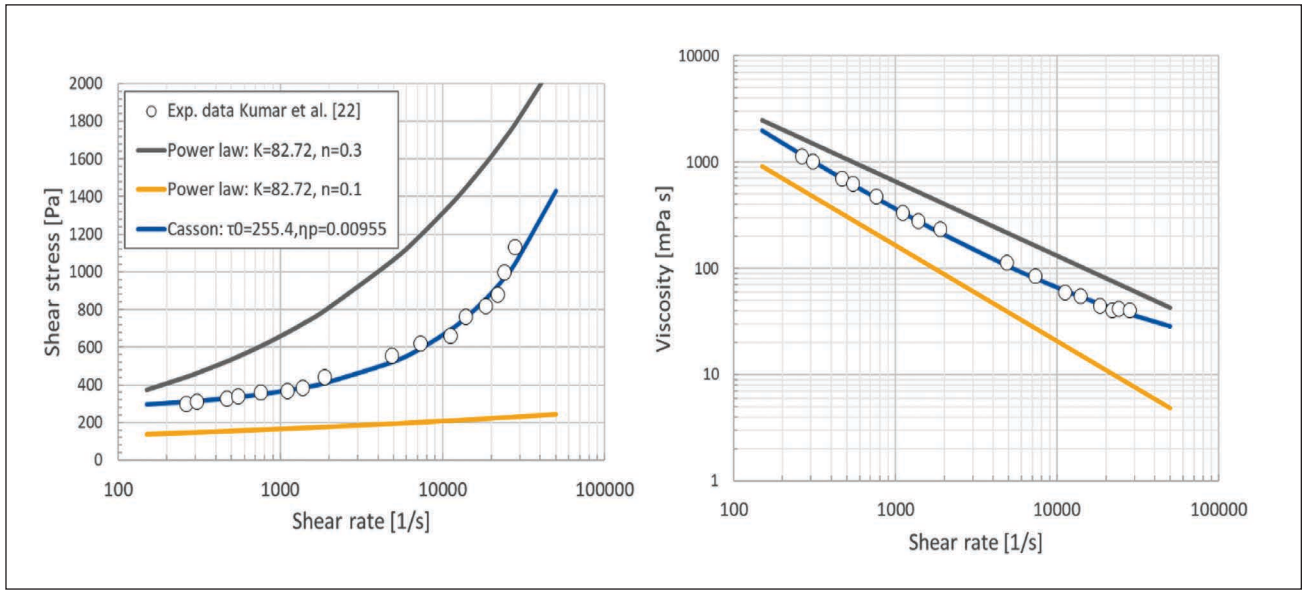

2. Fluid material models used in the simulations: the Casson material model fitted to, and the power law models enveloping, the experimental data by Kumar et al. [22]. Shear stress as a function of shear rate (left), and viscosity as a function of shear rate (right).

model equation provides a reasonable prediction of the rheological response of systems with yield stress and asymptotic viscosity at large shear rates. However, caution should be exercised while interpreting the results, as these models do not constitute time-dependent effects and cannot predict the thixotropic behavior of the fluid. Even though nanocellulosic materials at high consistencies are known to exhibit several flow heterogeneities such as shear banding and wall slip, those anomalies are assumed negligible here and are not modeled in this study. As it is challenging to compute the discontinuous material behavior of the solid regime (unyielded material), a bi-viscosity regularization model was adopted. The regularization assumes that the viscosity is substantial (η_0), albeit finite, when the fluid behaves as a solid ($\tau < \tau_0$). Beyond the yield stress ($\tau > \tau_0$), the viscosity of the fluid is determined by the rheological model in use.

INITIAL AND BOUNDARY CONDITIONS

The boundary conditions for the simulation domain are in Fig. 1. The no-slip and no-penetration boundary conditions were imposed on all the solid walls. At the inlet, a constant mass-flow rate is ensured by a fixed average inlet velocity (U_{in}). At the top and bottom outlets, the pressure is kept constant at atmospheric (P_{atm}) reference pressure. Moreover, the convective derivatives normal to the boundary interface for all the transported quantities are set equal to zero. On the rotating backing roller surface, a constant tangential velocity (U_r) was prescribed. Full wetting is assumed at all the walls and an equilibrium contact angle of θ=0 is used. There are two static contact lines where the fluid-free surface meets the die edge. A dynamic contact line is also present where the roller meets the free surface in the metered off zone. The contact angle boundary condition was utilized to correct the surface normal vector to adjust the interface's curvature near the wall. The coefficient of surface tension between the two phases was applied as σ=0.063 Nm^{-1}. The simulation was allowed to develop from the state where the coating fluid has completely filled the gap between the die lips and the backing roll. For the accuracy of computations, a dynamically adjusting time step was chosen so that the Courant number was maintained at less than 0.5. The simulations were also run for an extended period of 20 s to ensure the convergence of the model to a laminar steady state.

RESULTS AND DISCUSSION

Figure 3 shows the simulated coating flow for the base case with power law fluid (consistency index K=82.72 Pa $s^{0.3}$; power law index n=0.3), which has a slot-web gap (SWG) of 600 µm, slot die gap of 1000 µm, web speed of 10 m/min (0.167 m/s), and slot die average inflow rate of 0.180 m/s. At the slot gap exit, the flow is divided into upward and downward flows driven by the pressure from the feed into the slot die. The moving web creates an additional shear force to move material upward, and gravity helps to pull the metered off material down. There appears to be a vortex near the wetting front, and some air entrainment occurs near the substrate surface. However, any air is removed with the downward flow. The subfigure to the right in Fig. 3 shows the development of the velocity profile of the upward flow in the converging region between the upper slot die lip and the web. Here, the flow profile starts as a shear-dominated flow but gradually changes into a pressure driven flow, which is maintained up to the exit of the flow from under the upper slot lip. Due to the truncated parabolic flow profile created by the pressure-driven flow, the final wet coating layer thickness is ap-

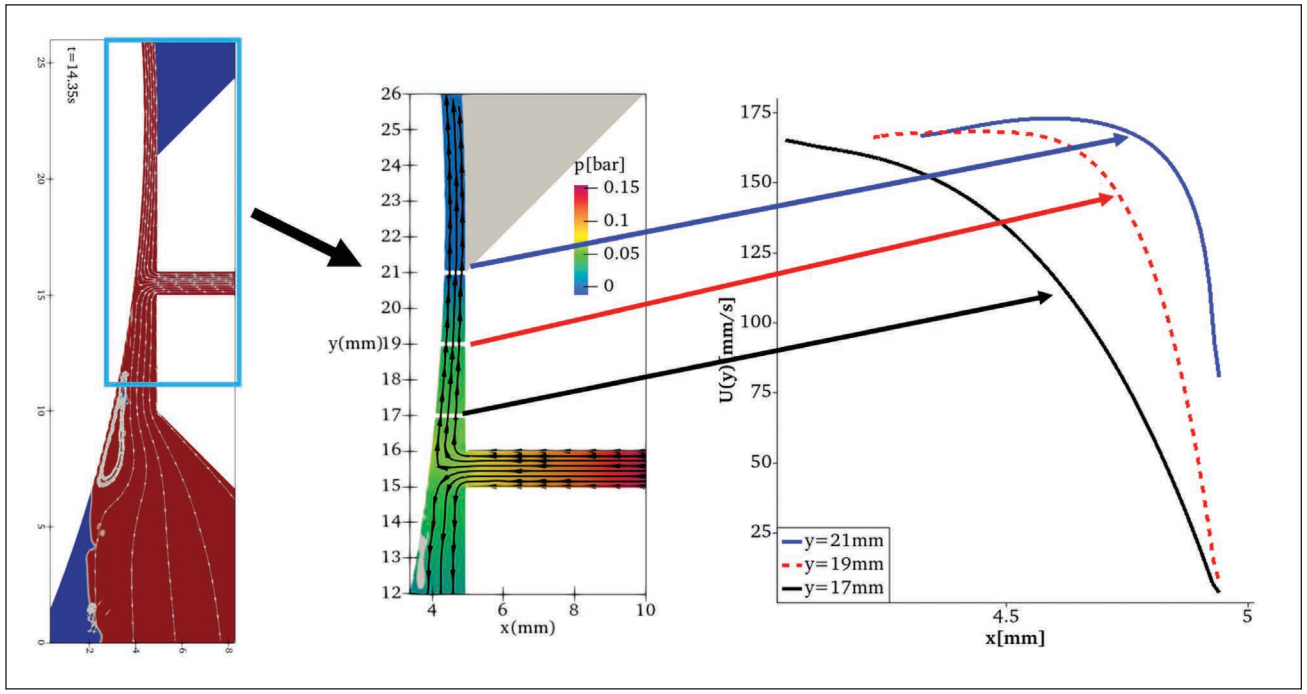

3. Slot die flow for a power law fluid (K = 82.72 Pa s0.3, n = 0.3) in the metering mode. A snapshot is given of the flow animation (left), pressure and streamline plot (middle), and flow profiles across the upward flow (right).

proximately the same as the SWG at the lip exit, 579 µm. With 3% concentration of CNF, this results in an approximately 18 g/m² (12 µm thick) dry coating layer. With these basic case parameters, 54% of the coating fluid fed into the coating head is predicted to end up on the substrate, and 46% is metered off. If the inlet average flow rate is increased by 50% to 0.270 m/s, the share of the coating being metered off increases to 62%, while the coating thickness increases by only 7% to 618 µm. The minimal change is due to the higher increase of the flow resistance for pressure driven flow in the narrow upward channel when compared to the slightly wider downward one. This is because the flow resistance in pressure driven flow scales to the third power of the gap. Due to the shear thinning rheology, the upward shear-flow induced by the moving substrate cannot overcome the pressure driven flow. Increasing the SWG to 1200 µm allows 100% of the coating to be applied on the substrate (no downward flow), resulting in wet coating thickness of 1103 µm in this case, whereas reducing the SWG to 300 µm leaves only 28% on the substrate for a wet coating thickness of 298 µm. The simulations confirm the practical experience that the wet coating thickness, and thereby the coat weight, can be controlled by the SWG and that changes in inlet flow rate do not considerably change the coated MFC amount in the metering operational mode of a slot die. The ability to maintain a constant coat weight while increasing the inlet flow rate can be beneficial in breaking down any flocculated structures in the nanocellulose suspension.

If the basic case power law fluid (K=82.72 Pa $s^{0.3}$, n=0.3) is replaced by a Newtonian fluid, the metered off share of the coating increases, resulting in a final wet coat weight of 482 µm, a reduction of 17% (**Table I**). If the power law index is reduced to n=0.1, the coat weight increases by 14% to 660 µm. These changes are a reflection of the changing flow profile between the slot die upper lip and the sub-

Fluid Model	Equation	Percentage Coated	Percentage Metered Off	Wet Coating Thickness
Power law	K=82.72 Pa $s^{0.3}$, n=0.3	54%	46%	579 µm
Newtonian	μ=0.1 Pa s	44%	56%	482 µm
Power law	K=82.72 Pa $s^{0.1}$, n=0.1	61%	39%	660 µm
Casson	τ_0=255.4 Pa, η_p=0.00955 Pa s	59%	41%	643 µm

I. Predicted coated and metered-off coating percentages, along with wet coating thicknesses for a constant inlet feed volumetric flow rate of 0.180 m/s, slot-web gap (SWG) = 600 µm, slot die gap = 1000 µm, and web speed 10 m/min.

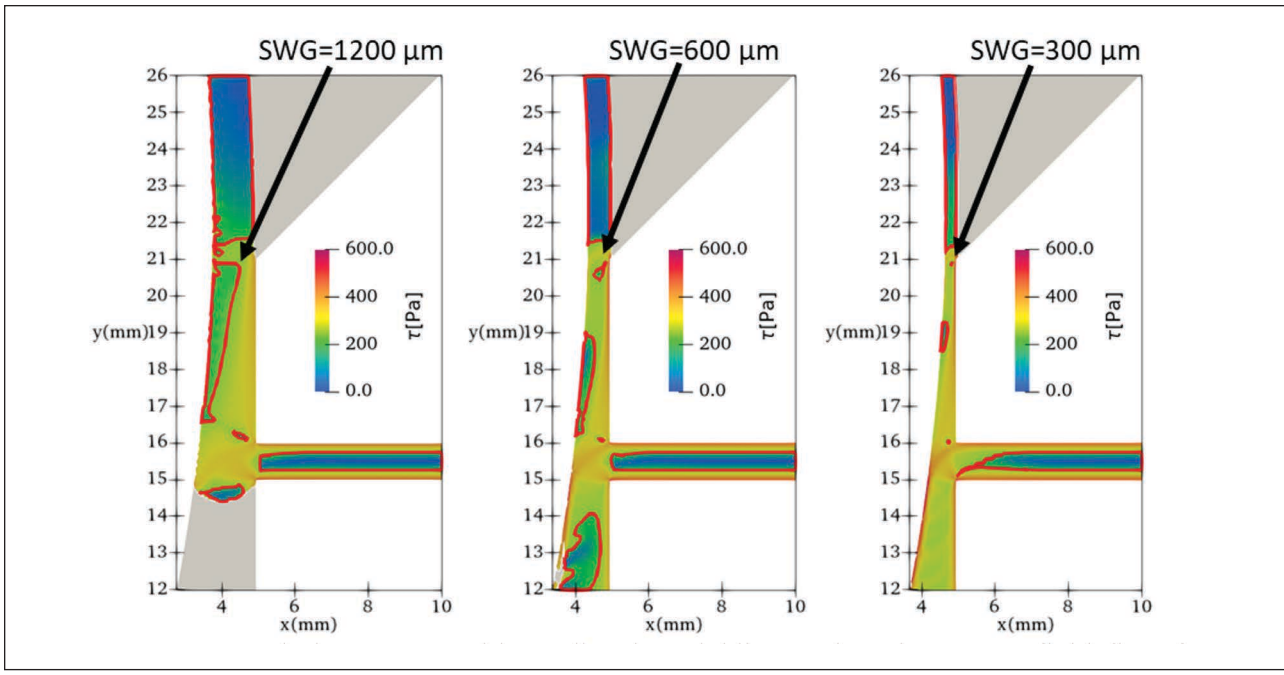

4. Local shear stress with predicted unyielding regions in Casson fluid flow for decreasing slot-web gap (SWG). Other parameters are as in Fig. 3.

strate. Shear flow that leads to contraction of the wet coating layer after the exit from under the coating head is promoted by reduced shear thinning behavior, i.e., a higher power law index. A low power law index leads to plug flow and can even lead to a partial extrusion of the coating from the slot lip exit.

One of the challenges of processing nanocellulose materials into coatings is their high yield stress. Although the apparent shear thinning behavior of nanocellulose can be mathematically modeled with the power law, it does not reflect the true microscopic behavior of the material. It is clear that if the local shear stress is lower than the yield stress of the material, the result is unyielded regions in the flow. In pipe and narrow gap flows, this leads to a nondeforming plug in the middle of the geometry. In the current work, we used the simplest material model that includes yield stress, the Casson model (plastic viscosity η_p=0.00955 Pa s, yield stress τ_0=255.4 Pa). **Figure 4** shows the shear stress distribution when modeling the nanocellulose suspension as the Casson fluid. The regions in the flow where the local shear stress is lower than the yield stress are highlighted in bright red. Both upward and downward regions are predicted to have unyielded areas, which can lead to coatability issues seen in experiments. Reducing the SWG decreases the unyielded areas, because overall shear stress levels increase between the substrate and the coating head. The unyielded plug in the middle of the slot gap is not influenced, because the inlet flow rate is kept constant. Although not simulated in the current work, it is clear that unyielded regions are bound to exist in the distribution channel of the slot die coating head. This is because the pressure drop, and thereby the shear stress, in the distribution channel is much lower than in the slot die gap by design. A typical design goal is to generate a 100-fold pressure drop in the slot die gap to ensure a uniform cross machine flow profile. This highlights the need to generate high enough shear stresses both within the coating head and in the application and metering areas. The challenge of overcoming the yield stress, which strongly depends on the fibril concentration, τ_0~O(Conc^3), is even more acute when trying to increase the nanocellulose concentration in order minimize the amount of water to be dried [21].

CONCLUSIONS

The current work developed a computational framework for numerical simulation of nanocellulosic materials with slot die coating. Simulations agreed with the experimentally demonstrated operation of the slot die in the unconventional metering mode. Flow dynamics of three types of fluids—Newtonian, power law, and Casson—were analyzed. Considerable differences in pressure fields and flow profiles were observed. The Casson model, which includes a yield stress parameter, demonstrated stagnation regions in flow that are not captured with the power law model. The unyielding regions can potentially lead to coatability issues, such as intermittent flow and fractures in the coating layer, that have also been seen in coating experiments. The results suggest that the power law model might not be sufficient to describe nanocellulose materials and that a model that includes a yield stress parameter should be considered. Future work will

need to verify the numerical simulation model with experiments. In this regard, there is also a need to obtain a better rheological characterization of nanocellulosic materials, especially at high concentrations and deformation rates. The importance of boundary slip, thixotropy, and elasticity for the coating flow needs to be evaluated, and the simulation model needs to be appropriately refined. The influence of substrate properties and clogging of slot entrance with fibrous material and three-dimensional effects of flow should be explored. The simulation parameter space for the current work was chosen to reflect earlier laboratory scale experimental coating studies. In the future, simulations with parameters relevant for high-speed industrial processes should be carried out. The feasibility of slot die operation in metering mode should be evaluated against short, pulled curtain mode. The simulation model developed here can find uses in the design of suitable coating apparatus (coating heads) to scale up future processes that target the production of nanocellulose coatings, films, and other products. **TJ**

ABOUT THIS PAPER

Cite this article as:
Kutty, F.P.A., Koppolu, R., Swerin, A., et al., *TAPPI J.* 19(11): 575(2020). https://doi.org/10.32964/TJ19.11.575

DOI: https://doi.org/10.32964/TJ19.11.575

ISSN: 0734-1415

Publisher: TAPPI Press

Copyright: ©TAPPI Press 2020

About this journal

ACKNOWLEDGMENTS

The authors would like to acknowledge postdoctoral financial support from KSLA through the Sweden-Finland bilateral "Tandem Forest Values" grant TFV I 2018 for the project "SimNano—Numerical simulation of coating processes for nanocellulosic materials."

ABOUT THE AUTHORS

We studied this topic because the fundamental understanding of nanocellulose flow behavior in coating processes is currently lacking. This research complements the previous experimental work on roll-to-roll slot die coating of nanocellulose on paperboard. In this work, the approach is to use mathematical modeling and numerical simulations.

The most difficult aspect of this study was to obtain reliable rheological data in order to define the material model for the simulations. We used existing data from a previous publication and complemented it with reasonable parameters based on reports in literature.

We discovered that unyielded regions can exist near the high shear regions, because the local gradient can drop to zero while the pressure-driven flow switches to shear-dominated flow. Our most interesting finding was the dominance of the pressure-driven flow in contrast to shear flow in the coating head-paper gap.

For mills, nanocellulose coating can be feasible on a large scale if the high yield stress of the material can be overcome by designing appropriate coating heads. Numerical simulation tools can be a great help here.

We are currently working on obtaining better quality rheological data for the nanocellulose material model at high shear rates and high solids contents. The numerical model will be verified against experiments and complemented to include boundary slip. After this effort, simulations at higher web speeds that are more relevant to industrial applications will be carried out.

Kutty is post-doctoral researcher, Koppolu is doctoral researcher, and Toivakka is professor in the Laboratory of Natural Materials Technology at Åbo Akademi University, Turku, Finland. Swerin is professor in the Department of Engineering and Chemical Sciences at Karlstad University, Karlstad, Sweden. Lundell is professor in the Linné FLOW Centre & Wallenberg Wood Science Center at KTH Royal Institute of Technology, Stockholm, Sweden. Email Toivakka at Martti.Toivakka@abo.fi.

Kutty

Koppolu

Swerin

Lundell

Toivakka

LITERATURE CITED

1. Osong, S.H., Norgren, S., and Engstrand, P., *Cellulose* 23(1): 93(2016). https://doi.org/10.1007/s10570-015-0798-5.
2. Kargarzadeh, H., Ioelovich, M., Ahmad, I., et al., *Handbook of Nanocellulose and Cellulose Nanocomposites*, Wiley-VCH Verlag, Weinheim, 2017, pp. 1-47. https://doi.org/10.1002/9783527689972.ch1.
3. Kumar, V., Bollström, R., Yang, A., et al., *Cellulose* 21(5): 3443(2014). https://doi.org/10.1007/s10570-014-0357-5.
4. Chinga-Carrasco, G., *Nanoscale Res. Lett.* 6(1): 417(2011). https://doi.org/10.1186/1556-276X-6-417.
5. Abitbol, T., Rivkin, A., Cao, Y., et al., *Curr. Opin. Biotechnol.* 39(I): 76(2016). https://doi.org/10.1016/j.copbio.2016.01.002.
6. Kargarzadeh, H., Huang, J., Lin, N., et al., *Prog. Polym. Sci.* 87: 197(2018). https://doi.org/10.1016/j.progpolymsci.2018.07.008.
7. Ventura, C., Pinto, F., Lourenço, A.F., et al., *Cellulose* 27(10): 5509(2020). https://doi.org/10.1007/s10570-020-03176-9.
8. Ferrer, A., Pal, L., and Hubbe, M., *Ind. Crops Prod.* 95: 574(2017). https://doi.org/10.1016/j.indcrop.2016.11.012.
9. Silva, F.A.G.S., Dourado, F., Gama, M., et al., *Nanomaterials* 10(10): 2041(2020). https://doi.org/10.3390/nano10102041.
10. Syverud, K. and Stenius, P., *Cellulose* 16(1): 75(2009). https://doi.org/10.1007/s10570-008-9244-2.
11. Tayeb, A.H., Tajvidi, M., and Bousfield, D., *Molecules* 25(6): 1344(2020). https://doi.org/10.3390/molecules25061344.
12. Lavoine, N., Desloges, I., Khelifi, B., et al., *J. Mater. Sci.* 49(7): 2879(2014). https://doi.org/10.1007/s10853-013-7995-0.
13. Mazhari Mousavi, S.M., Afra, E., Tajvidi, M., et al., *Progr. Org. Coat.* 122: 207(2018). https://doi.org/10.1016/j.porgcoat.2018.05.024.
14. Shanmugam, K., Varanasi, S., Garnier, G., et al., *Cellulose* 24(7): 2669(2017). https://doi.org/10.1007/s10570-017-1328-4.
15. Mazhari Mousavi, S.M., Afra, E., Tajvidi, M., et al., *Cellulose* 24(7): 3001(2017). https://doi.org/10.1007/s10570-017-1299-5.
16. Koponen, A.I., *Cellulose* 27(4): 1879(2020). https://doi.org/10.1007/s10570-019-02908-w.
17. Guezennec, C., Girard, F., Dufresne, A., et al., *Rev. ATIP* 70: 6(2016).
18. Svending, P., Kritzinger, J., Phipps, J., et al., "Development of corrugated board surfaces suitable for water intensive printing," *TAPPI PaperCon*, TAPPI Press, Peachtree Corners, GA, USA, 2018.
19. Chowdhury, R.A., "Roll-to-roll fabrication of cellulose nanocrystal nanocomposite for gas barrier and thermal management applications, " Ph.D. thesis, Purdue University, West Lafayette, IN, USA, 2019.
20. Kumar, V., Elfving, A., Koivula, H., et al., *Ind. Eng. Chem. Res.* 55(12): 3603(2016). https://doi.org/10.1021/acs.iecr.6b00417.
21. Nazari, B., Kumar, V., Bousfield, D.W., et al., *J. Rheol.* 60(6): 1151(2016). https://doi.org/10.1122/1.4960336
22. Kumar, V., Nazari, B., Bousfield, D.W., et al., *Appl. Rheol.* 26(4): 1(2016).
23. Kontturi, E., Tammelin, T., and Österberg, M., *Chem. Soc. Rev.* 35(12): 1287(2006). https://doi.org/10.1039/B601872F.
24. Saarikoski, E., Saarinen, T., Salmela, J., et al., *Cellulose* 19(3): 647(2012). https://doi.org/10.1007/s10570-012-9661-0.
25. Akbarzadeh, V. and Hrymak, A.N., *AIChE J.* 62(6): 1933(2016). https://doi.org/10.1002/aic.15187.
26. Carvalho, M.S. and Kheshgi, H.S., *AIChE J.* 46(10): 1907(2000). https://doi.org/10.1002/aic.690461003.
27. Deshpande, S.S., Anumolu, L., and Trujillo, M.F., *Comput. Sci. Discovery* 5(1): 014016(2012). https://doi.org/10.1088/1749-4699/5/1/014016.
28. Hirt, C.W. and Nichols, B.D., *J. Comput. Phys.* 39(1): 201(1981). https://doi.org/10.1016/0021-9991(81)90145-5.